BM@N Analysis Note

Baryonic femtoscopy in 3.2 A GeV argon-nucleus interactions

Analysis team: P.Alekseev, L.Kovachev, R.Lednicky, V.Plotnikov, N.Pukhaeva, T.Ribakov, A.Stavinskiy, N.Zhigareva

Abstract
A motivation for the baryon femtoscopy at the energy range of the experiment Baryonic Matter at the Nuclotron (BM@N) is discussed. The BM@M results on the proton-proton and proton-deuteron femtoscopy in the interactions of the argon beam of 3.2 AGeV kinetic energy with the *C, Al, Cu, Sn, Pb* targets are presented. The analysis procedure is described in detail. The dependence of the *pp* and *pd* correlation functions on the particle momentum in the pair rest frame has been obtained in the center-of-mass rapidity range of 0±0.6 and compared with the theoretical calculations. The fitted source size parameters are compared with the available data.

1. Physical motivation for baryon femtoscopy

The study of momentum correlations at small relative momenta of particles in their center-of-mass system (correlation femtoscopy) allows one to get the information on the space-time characteristics of the particle production process on the femtometer scale (as reflected in the name of the method) due to the effects of final state interaction (FSI) and quantum statistics (QS).

The information obtained by this method supplements the information about the production process obtained with the help of other observables. The choice of the studied production process, the species of correlated particles, the kinematic range and the required measurement accuracy depend on the task to be solved by the femtoscopy.
In the Nuclotron kinetic energy range of a few GeV per nucleon, the baryons are the dominant particle species, so the baryon femtoscopy is primarily relevant.

The models used to describe the nuclear interactions focus on the description of inclusive cross sections, flows, fluctuations, etc. A study of the particle correlations is often ignored, although it can significantly refine models, in particular, the mechanism of the fragment formation.

One of the unsolved fundamental problems of high-energy physics remains the description of the hadronization process. The experimental data at ultra-high energies are not required to solve this problem since the typical energy-momentum transfers during the hadronization process do not exceed several hundreds of MeV. Moreover, the nuclear collisions at relatively low and ultra-high energies complement each other well, since the excited hadronizing matter is characterized by a large net baryonic charge in the first case, contrary to nearly zero net baryonic charge in the second case.

Some features of the hadronization process may have different model interpretation. For example, an increase in the fraction of baryons (especially strange baryons) in collisions of relativistic nuclei is expected due to the formation of quark-gluon plasma, as well as, in the popular Lund model - due to the formation of so-called “ropes” of closely spaced strings. Then, the creation of (strange) baryons is expected from a region of a small transverse size, which may significantly differ from the predictions of other models and can be tested with the help of femtoscopic measurements.

The space-time picture measured by two-particle femtoscopy in terms of the effective source radius

$$r_0 = \sqrt{(r_{01}^2 + r_{02}^2)/2} r_0 = \sqrt{(r_{01}^2 + r_{02}^2)/2}$$

is influenced not only by the different source radii $r_{0i} r_{0i}$ of different particles but, in case of a complex production process characterized by several radii, also by the different sensitivity of the strong FSI, Coulomb FSI and QS to the small and large radii. Therefore, it is important to study two-particle femtoscopic correlations with various particle species, particularly, in various pairs of protons, neutrons and hyperons.

There are data in the literature on the source sizes from the pp and pΛ femtoscopic correlations in a wide energy range of the colliding nuclei (see, e.g., [2-5]). They do not contradict to the expected decrease of the source size for the events with the strangeness creation, but they are not sufficient for certain conclusions.

The study of pd correlations is not only interesting in itself. It also allows us to obtain the information necessary for further steps to improve the efficiency of the algorithms used in BM@N to treat charged particles with close momenta.

We start this program from pp and pd femtoscopy. The development of the BM@N detector due to the commissioning of new detectors, software improvements and the development of the accelerator complex will allow us to continue this program including strange and neutral particle femtoscopy.

2. Femtoscopy formalism

In a production process of a small enough phase space density (which is usually the case even in heavy-ion collisions) the correlations of two particles emitted with nearly equal four-velocities p1/M1 and p2/M2 are dominated by their mutual final state interaction (FSI) and, in case of identical particles, also by the symmetrization requirement of quantum statistics (QS).

The ideal two-particle correlation function is defined as the ratio of a number of pairs of correlated particles with the three-momenta in the bins around given $\mathbf{p_1}$ and $\mathbf{p_2}$ divided by a

number of particle pairs with the switched off the effects of FSI and QS, normalized to unity at sufficiently large relative momenta [1,6]:

$$R(\mathbf{p_1}; \mathbf{p_2}) = N(\mathbf{p_1}; \mathbf{p_2})/N_0(\mathbf{p_1}; \mathbf{p_2}). \qquad (2.1)$$

Often, the six-dimensional correlation function is projected to the three- or one-dimensional ones and studied at given transverse momentum and rapidity intervals as functions of half the relative momentum $\mathbf{k}^* = \mathbf{p_1}^* = -\mathbf{p_2}^*$ or $k^* = |\mathbf{k}^*|$ in the pair rest frame (PRF, denoted by *).

In the absence of any correlations, the number of pairs of uncorrelated particles reduces to a product of single particle numbers: $N_0(\mathbf{p_1}; \mathbf{p_2}) = N(\mathbf{p_1})\, N(\mathbf{p_2})$ and $R(\mathbf{p_1};\mathbf{p_2}) = 1$. The product of the single particle numbers is usually assumed in Eq. (2.1) to construct the experimental correlation function despite it neglects the dynamical and kinematical correlations present in the numerator.

The construction of such a correlation function is rather involved and requires large statistics. In fact, following Ref. [1], the denominator in Eq. (2.1) is often obtained by mixing particles from different events of a given class and the experimental correlation function is determined as:

$$R_{exp}(\mathbf{p_1}; \mathbf{p_2}) = N(\mathbf{p_1}; \mathbf{p_2})/N_{mix}(\mathbf{p_1}; \mathbf{p_2}). \qquad (2.2)$$

The use of the mixing method greatly simplifies the analysis, since the factoring part of the detector efficiency cancels out in the correlation function. However, the non-factoring component of efficiency, especially the effects associated with the particle tracks almost coinciding in both space and time, must be studied.

Mixed events lack not only FSI and QS correlations, but also all other momentum correlations, for example, due to the energy-momentum conservation, sequential resonance or fragment decays, contribution of the processes with different single-particle spectra (e.g., due to a mixture of collisions with different impact parameters), etc. These correlations are rather complex but quite wide or weak at small relative momenta. If necessary, they are taken into account, e.g., by polynomial corrections.

The experimental correlation function can be affected also by the admixture of misidentified particles or particles from long-lived emitters [7]. Thus, assuming that the true correlation function R is observed only in a fraction λ of the pairs, while $R = \tilde{R}\tilde{R} = 1$ for the remaining fraction $1-\lambda$, one arrives at the experimental correlation function:

$$R_{exp} = N[(1-\lambda) + \lambda R], \qquad (2.3)$$

where N is a free normalization parameter.

Often, a possible deviation from unity of the so-called residual correlation functions $\tilde{R}\tilde{R}_i$ [8–10] contributing to the fraction $(1-\lambda) = \Sigma_i \lambda_i$ of "uncorrelated" pairs is taken into account, modifying Eq. (2.4) by the substitution $(1-\lambda) \rightarrow\rightarrow \Sigma\lambda_i \tilde{R}\tilde{R}_i$.

Also, a momentum dependence is sometimes introduced in the normalization

factor *N* to account for possible long-range momentum correlations.

A detailed description of the correlation function calculation is given in Appendix 1. These calculations assume that

- the single-particle spectra are sufficiently smooth in a narrow region of the correlation effect (smoothness assumption);
- the production time of the particles is much shorter than their interaction time in the final state;
- the contribution of multiparticle states with small relative particle velocities is negligible due to a small or moderate phase-space density of produced particles;
- the spin and isospin projections are equilibrated;
- the separation *r*-distribution is reasonably described in terms of simple Gaussian parameterizations with the radius parameter r_0.

The calculated pp and pd correlation functions for different values of the radius parameter r_0 are presented in Fig. 2.1

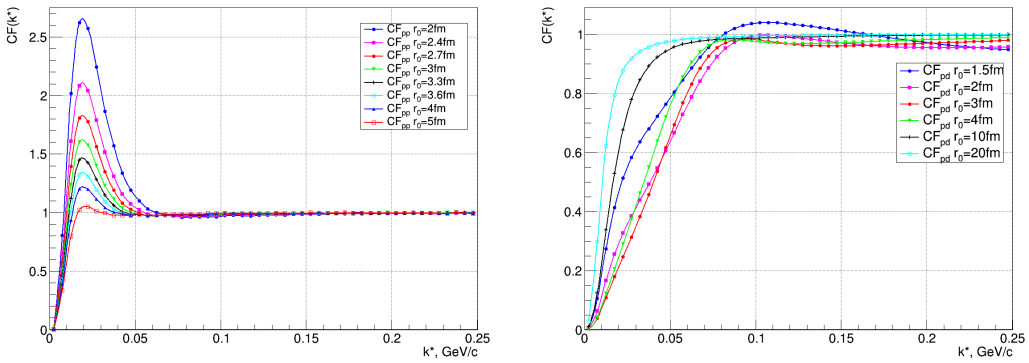

pp pd

Fig.2.1 The calculated pp (left) and pd (right) correlation function for different values of the radius parameter r_0

3. BM@N configuration in the argon beam run and the run conditions

In the next two paragraphs (detector structure and identification of protons and deuterons), we selectively cite [11], where these issues are described in detail and references are given to the characteristics of individual detectors. A brief repetition is given below for the reader convenience.

The BM@N detector is a forward spectrometer covering the pseudorapidity range $1.6 \leq \eta \leq 4.4$. A schematic view of the BM@N setup in the argon-beam run is shown in Fig. 3.1. The research program is devoted to measurements of inelastic collisions of the *Ar* beam of the kinetic energy of 3.2 AGeV with different targets: *C, Al, Cu, Sn, Pb*.

The spectrometer includes a central tracking system consisting of 3 planes of forward silicon-strip detectors (ST) and 6 planes of detectors based on gas electron multipliers (GEM). The central tracking system is located downstream of the target region inside of a dipole magnet with a bending power of about 2.1 Tm and with a gap of 1.05 m between the poles. In the measurements reported here, the central tracker covered only the upper half of the magnet acceptance.

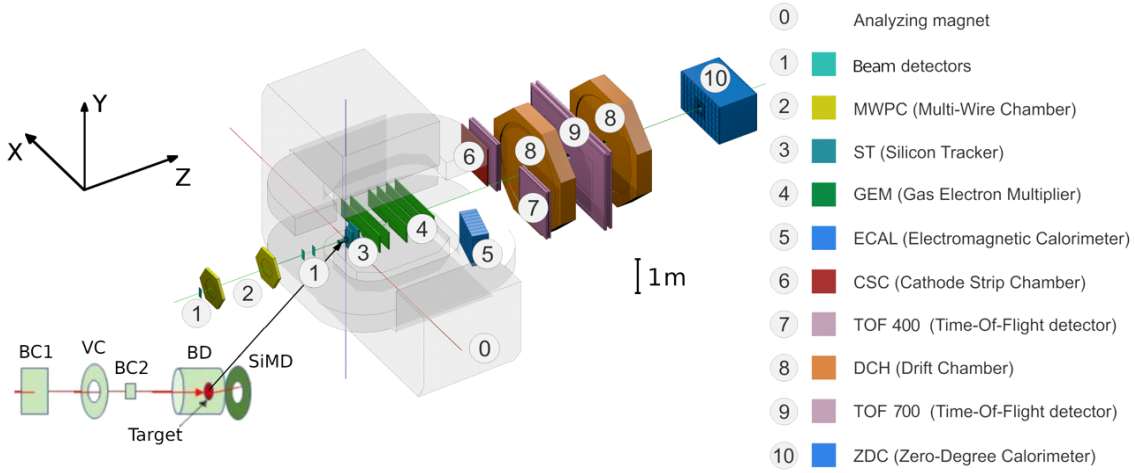

Figure 3.1 Schematic view of the BM@N setup in the argon beam run.

Two sets of drift chambers (DCH), a cathode strip chamber (CSC), two sets of time-of-flight detectors (ToF), and a zero-degree calorimeter (ZDC) are located downstream of the dipole magnet. The tracking system measures the momentum of charged particles with a relative uncertainty that varies from 2.5% at a momentum of 0.5 GeV/c to 2% at 1 – 2 GeV/c and rises linearly to 6.5% at 5 GeV/c. The time resolutions of the ToF-400 and ToF-700 systems are 84 ps and 115 ps, respectively.

Two beam counters (BC1, BC2), a veto counter (VC), a barrel detector (BD) and a silicon multiplicity detector (SiMD) are used for the event triggering and for the measurement of the incoming beam ions. The BC2 counter also provides the start time T0 for the time-of-flight measurement. The BD detector consists of 40 azimuthal scintillating strips arranged around the target, and the SiMD detector consists of 60 azimuthal silicon segments situated behind the target.

Data were collected with an argon beam intensity of a few 10^5 ions per spill and a spill duration of 2–2.5 sec. The kinetic energy of the beam was 3.2 A GeV with a spread of about 1%. A set of solid targets of various materials (C, Al, Cu, Sn and Pb) with an interaction length of 3% was used. The experimental data correspond to a total integrated luminosity of 7.8 μb^{-1} collected with the different targets: 2.1 μb^{-1} (C), 2.3 μb^{-1} (Al), 1.8 μb^{-1} 1 (Cu), 1.1 μb^{-1} (Sn), 0.5 μb^{-1} (Pb).

A total of 16.3 M argon-nucleus collisions at 3.2 AGeV were reconstructed. To count the number of beam ions that passed through the target, a logical beam trigger BT=BC1∧VC∧BC2 was used. The following logic conditions were applied to generate the trigger signal:

1) BT∧(BD≥ 3, 4);
2) BT∧(SiMD≥ 3, 4);
3) BT∧(BD≥ 2)∧(SiMD≥ 3).

The trigger conditions were varied to find the optimal ratio between the event rate and the trigger efficiency for each target. Trigger condition 1 was applied for 60% of the data collected with the carbon target. This trigger fraction was continuously reduced with the atomic weight of the target down to 26% for the Pb target. The fraction of data collected with trigger condition 2 was increased from 6% for the carbon target up to 34% for the Pb target. The rest of the data was collected with trigger condition 3.

4. Event reconstruction, p and d selection criteria

Track reconstruction in the central tracker is based on a "cellular automaton" approach implementing a constrained combinatorial search of track candidates with their subsequent fitting by a Kalman filter to determine the track parameters.
These tracks are used to reconstruct primary and secondary vertices as well as global tracks by extrapolation and matching to hits in the downstream detectors (CSC, DCH and ToF).
The primary collision vertex position (PV) is measured with a resolution of 2.4 mm in the X–Y plane perpendicular to the beam direction and 3 mm in the beam direction.
Charged particles (protons, deuterons and tritons) are identified using the time of flight Δt measured between T0 and the ToF detectors, the length of the trajectory Δl, and the momentum p reconstructed in the central tracker. Then the squared mass M^2 of the particle is calculated as: $M^2 = p^2[(\Delta tc/\Delta l)^2 - 1]$, where c is the speed of light.
The following criteria are required for selecting proton, deuteron and triton candidates:
• Each track has at least 4 hits in the GEM detectors (6 detectors in total).
Hits in the forward silicon detectors are used to reconstruct the track, but no requirements are applied to the number of hits.
• Tracks originate from the primary vertex. The deviation of the reconstructed vertex Zver from the nominal target position along the beam direction Z0 is limited to -3.4 cm < Zver − Z0 < 1.7 cm. The upper limit corresponds to ~5.7σ of the Zver spread and it cuts off interactions with the trigger detector located 3 cm behind the target. The beam interaction rate with the trigger detector is well below 1% and was not simulated since it does not affect the precision of the Monte Carlo simulation.
• Distance from the track to the primary vertex in the X–Y plane at Zver (DCA) is required to be less than 1 cm, which corresponds to 4σ of the vertex residual distribution in the X–Y plane.
• Momentum range of positively charged particles is limited by the acceptance of the ToF-400 and ToF-700 detectors to p > 0.5 GeV/c and p > 0.7 GeV/c, respectively.
• Distance of extrapolated tracks to the CSC (DCH) hits as well as to the ToF-400 (ToF-700) is required within 2.5σ of the momentum dependent hit-track residual distributions.

The mass squared (M^2) spectra of positively charged particles produced in interactions of the 3.2 A GeV argon beam with various targets are shown in figures 4.1 for ToF-400 (left) and ToF-700 (right) data, respectively. Only particles satisfying the above selection criteria contribute to these spectra.

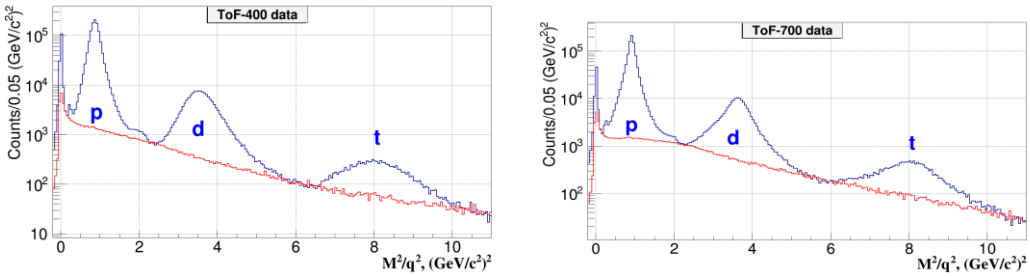

Figure 4.1 The M^2/q^2 spectra of the particles of a positive charge q produced in argon nucleus interactions, measured in the ToF-400 (left) and ToF-700 (right) detectors.

Peaks of protons, deuterons and tritons with the charge q = 1 are indicated; the small peaks of He fragments with q = 2 either overlap with the deuteron one (4He) or show up at M2/q2 ~ 2 (GeV/c2)2 (3He). The red histograms show the background estimated from the "mixed events". The shape of the background under the proton, deuteron and triton signals in the M^2/q^2 spectra is estimated using the "mixed event" method. For that, the tracks reconstructed in the central tracker are matched to hits in the ToF detectors taken from different events containing a similar number of tracks. The "mixed event" background is normalized to the integral of the signal histogram outside the M^2/q^2 windows of protons, deuterons and tritons. It is found that the background level differs for the light and heavy targets and for different intervals of rapidity and transverse momentum.

Selecting the M^2 range for protons

In order to select the proton M^2 range taking into account the rapidity selection, the M^2 distribution is constructed by calculating the rapidity for all particles as for protons and applying the selection to this rapidity value (fig.4.2).

The proton background is cut-off by a linear background function in the M^2 range [0.37, 1.45]. The vertical coordinates of the line points are calculated by averaging over five bins within the range. In this case, for the joint TOF-400 and TOF-700 distribution, the background composes 1.2% (348412 particles: 344265 protons, 4147 background).

Decreasing the M^2 range to [0.5, 1.3], the background decreases to 0.9% (347276 particles: 344191 protons, 3085 background). The final number of protons exceeds the initial one, since some points on the distribution tails are below the background line.

Below we summarize the results in the M^2 range [0.5, 1.3] for separate and joint TOF detectors:
TOF-400: 216784 particles, 1809 (0.83%) background, 214975 protons
TOF-700: 130492 particles, 1276 (0.98%) background, 129216 protons
2 x TOF: 347276 particles, 3085 (0.89%) background, 344191 protons

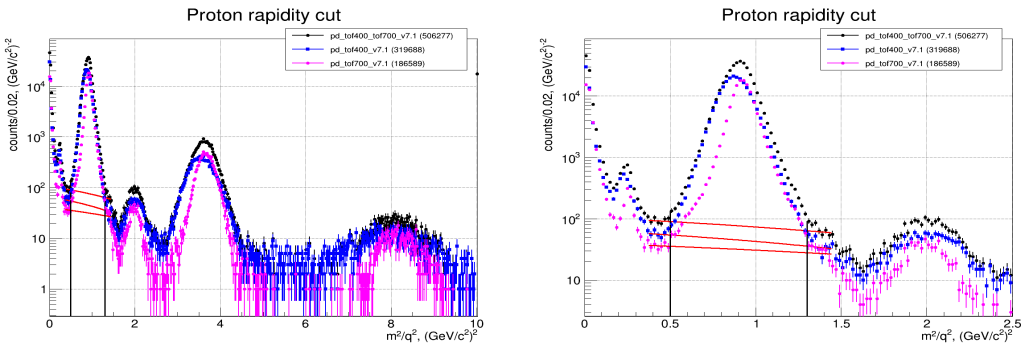

Fig.4.2 Selecting the M^2 range for protons

Selecting the M^2 range for deuterons

In order to select the deuteron M^2 range taking into account the rapidity selection, the M^2 distribution is constructed by calculating the rapidity for all particles as for deuterons and applying the selection to this rapidity value (fig.4.3).
The deuteron background is cut off by a linear background function in the M^2 range [2.5, 5.5]. The vertical coordinates of the line points are calculated by averaging over five bins within the range. In this case, for the joint distribution of TOF-400 and TOF-700, the background composes 6.1% (66793 particles: 62698 deuterons, 4095 background).
Reducing the M^2 range to [2.8, 4.5], the background decreases to 4.2% (64822 particles: 62102 deuterons, 2719 background).

Below we summarize the results in the M^2 range [0.5, 1.3] for separate and joint TOF detectors:
TOF-400: 39651 particles, 2270 (5.72%) background, 37381 deuterons
TOF-700: 25171 particles, 449 (1.79%) background, 24722 deuterons
2 x TOF: 64822 particles, 2719 (4.19%) background, 62103 deuterons

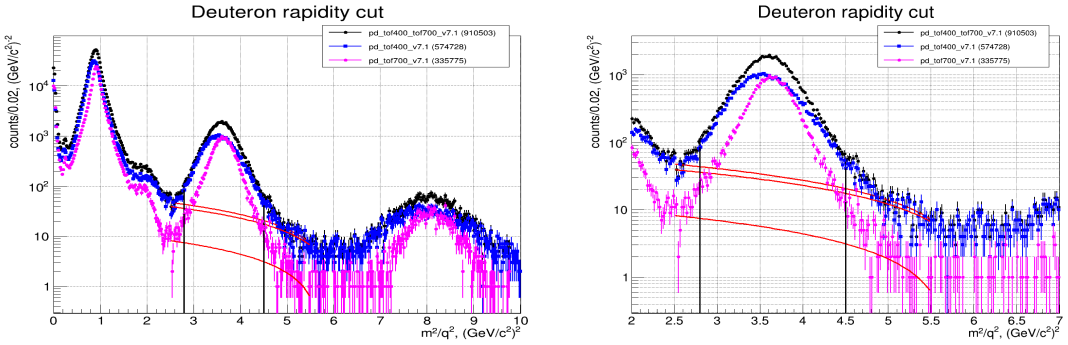

Fig.4.3 Selection of the M^2 range for deuterons

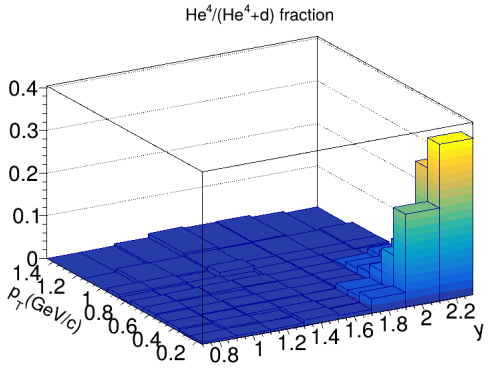

Fig. 4.4. The ^{4}He fraction in the ^{4}He + d sample measured in the rapidity vs. transverse momentum plane in Ar+A interactions

The proton and deuteron signals are extracted in M^2 windows, which depend on rapidity, and at the maximal rapidity extend from 0.4–1.7 $(GeV/c^2)^2$ and 2.3–5.0 $(GeV/c^2)^2$ respectively. We estimate the background as large as 10% for deuterons and a few % for protons.

The dE/dx information from the GEM detectors is used to separate the deuteron signals from the overlapping TOF ^{4}He signals. The fraction of ^{4}He in the total ^{4}He +d sample is determined in the rapidity and transverse momentum bins and subtracted from the deuteron TOF signals. Figure 4.4 shows the fraction of ^{4}He in the ^{4}He + d sample measured in the rapidity vs. transverse momentum plane in Ar+A interacions. In most of the y − pT bins, the ^{4}He fraction does not exceed 3%. However, in a few bins at large y and low p_T, it reaches 20–35%. For correlation measurements, we restrict rapidity range to 0.5-1.7, where the ^{4}He background is negligible.

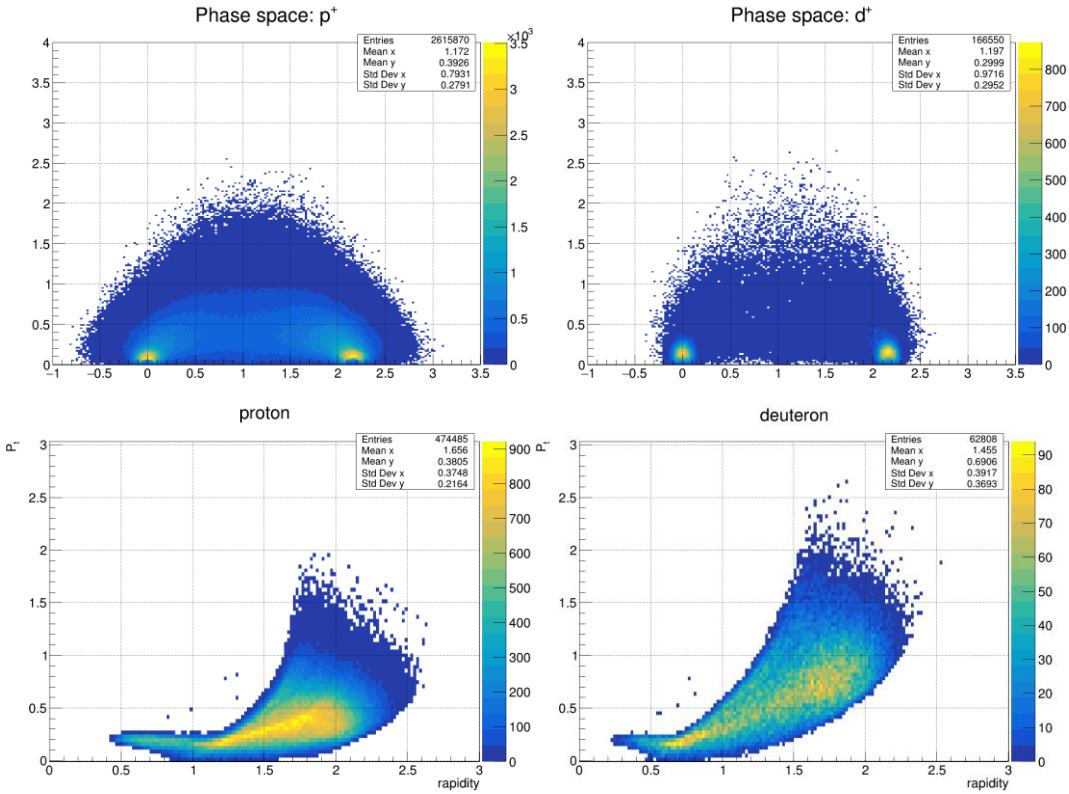

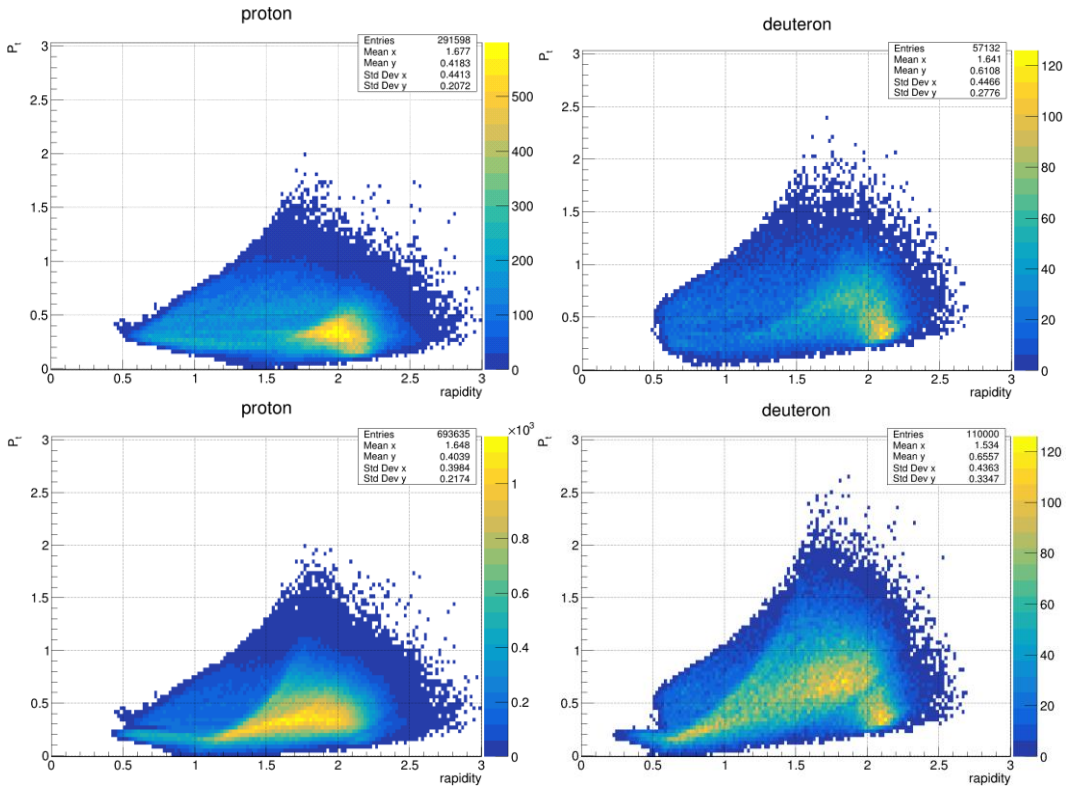

Fig.4.5. The p_T-y distribution for A+A interactions at 3.2AGeV. Up-to down: DCM-SMM model, within the **ToF-700** acceptance**,** within the **ToF-400** acceptance**,** within the **ToF-700+ToF-400** acceptance**; l**eft for protons, right for deuterons.

Figure 4.5 shows that the region of protons and deuterons with a rapidity of more than 1.7 is physically inhomogeneous: it contains both particles with small transverse momenta, where the momentum transfer from the incoming nucleus is relatively small, and particles with transverse momenta of the order of 1 GeV/c. The size of the region measured by femtoscopy significantly depends on the momentum transferred to protons and deuterons, so summing up statistics at forward rapidities without careful p_T selection is unjustified. This analysis is therefore limited to the central rapidities only.

To select events outside the area of intersection of the ToF-400 and ToF-700 detectors, a linear cut on the (px, pz) plane is used (Fig. 4.4). Events that meet the conditions below are discarded:
px >= 0.13333333 * pz - 0.37333333 for TOF-700,
px <= 0.13333333 * pz - 0.37333333 for TOF-400.
The above separation line mostly removes events from the TOF-700, while only a few events from the TOF-400 appear below this line, most likely due to the identification errors.

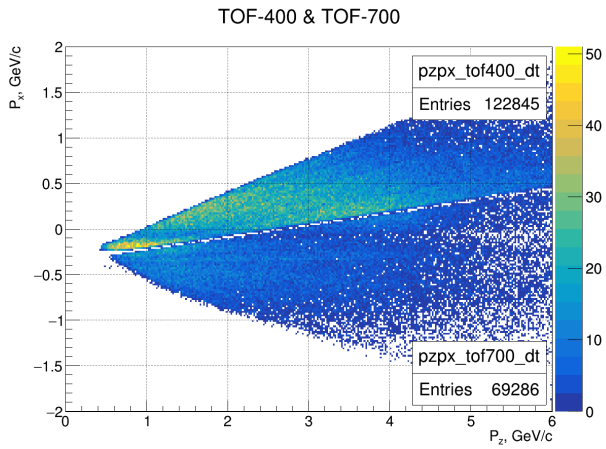

Fig.4.6

The correlation analysis uses two data samples with identified particles:
TOF-700 mini DST file Fragments_Ar_full_statistic.root
Number of identified particles 2,725,618
Number of events 2,104,627
Number of events with more than one particle 502,899

TOF-400 mini DST file Tof400_Data_sigma2_5_PCorr.root
Number of identified particles 2,238,836
Number of events 1,723,106
Number of events with more than 1 particle 422,432

Prior to the start the femtoscopic analysis, data is pre-selected on the quality of the GEM track, the position of the primary vertex and the number of tracks in it. In addition, events with fewer than two particles are excluded.

For TOF-700, the cutouts are applied:
Target number = 0 (empty target)
Z of the primary vertex outside the range [-3.4, 1.7]
In Silicon detectors < 1 hit
In GEM detectors < 4 hits
Less than 2 tracks in the primary vertex
DCH residuals outside the 2.5 sigma range
TOF-700 residual outside the 2.5 sigma range
Less than two tracks left in the event.
After cleaning, 415,577 particles remain in 190,441 events in TOF-700

For TOF-400, the cutouts are applied:
Target number = 0 (empty target)
Z of the primary vertex is outside the range [-3.4, 1.7]
In Silicon detectors < 1 hit
In GEM detectors < 4 hits
Less than 2 tracks in the primary vertex

Less than two tracks left in the event
In CSC and TOF-400 the sigma cutouts are applied in the source file.
After cleaning, 669,845 particles remain in 300,298 events in TOF-400

5. pd and pp momentum (k^*) distributions in PRF

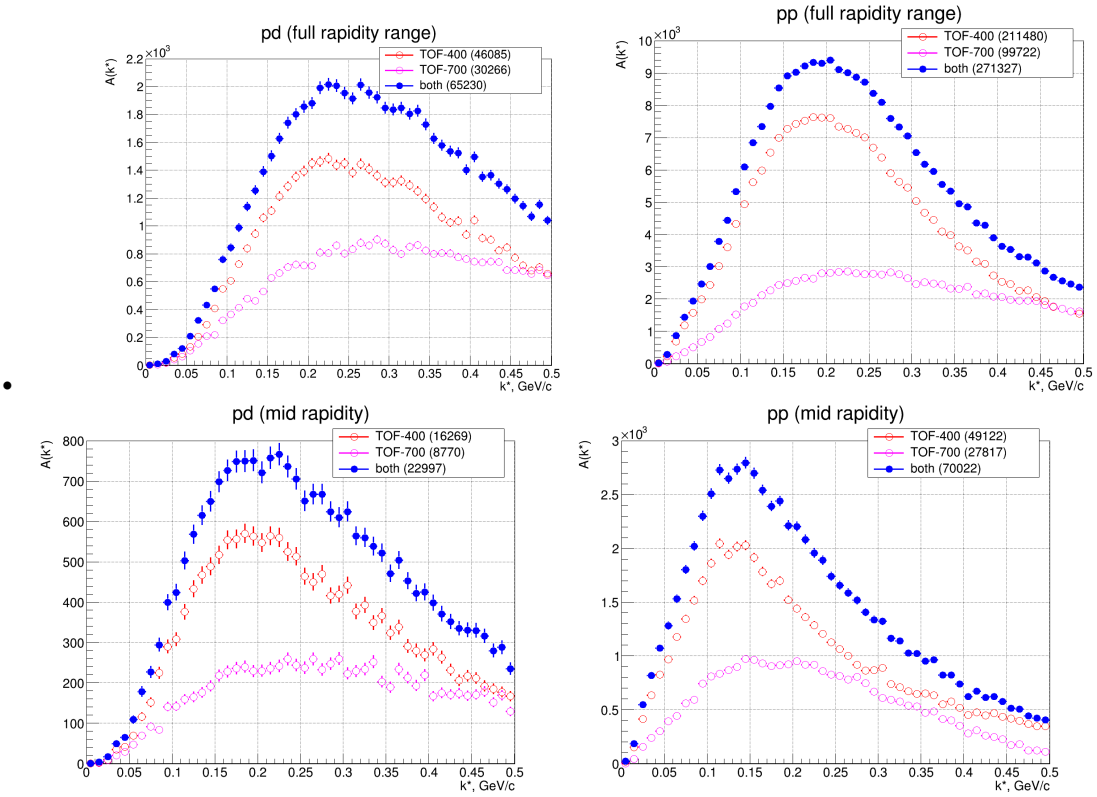

Fig.5.1 pd and pp momentum (k^*) distributions in PRF

6. Mixing procedure

• For each pair of particles in each event, k^* for the distribution A(k^*) $\equiv N \equiv N$ (k^*) is calculated and mixed distribution B(k^*) $\equiv N \equiv N_{\text{mix}}$($k^*$) is constructed. For mixing, one of the particles of the pair in a given event is taken and a search for the second particle in "similar" events is performed. The “similar” events and the constructed pairs should fulfill the following conditions:

• • the target material and the number of the studied particle species is the same as in a given event,

• • the k^* of the mixed pair falls within the studied interval (range of the histograms A(k*) and B(k*)).

The search for “similar” events is performed until:
• the specified number of mixed pairs satisfying the search conditions has been reached,

• all the available events have been used.
If the number of the found mixed pairs is less than the specified minimum number, then they are considered statistically insignificant and skipped (neither the true pair nor the mixed pairs contribute to the respective distributions of A and B). Otherwise, the k^* values from the found mixed pairs are placed in the weighted histogram B(k*, 1/nmix) with the weight inverse to the number nmix of the found mixed pairs.

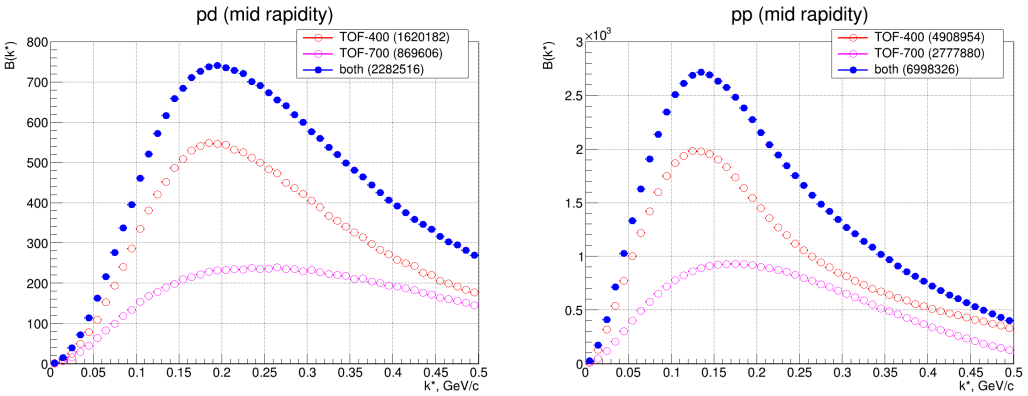

Fig. 6.1 The mixed pd (left) and pp (right) k* distributions in the central rapidity interval

7. The pd and pp correlation functions

The experimental pd and pp correlation functions in the midrapidity interval are shown in Figs. 7.1 and 7.2.

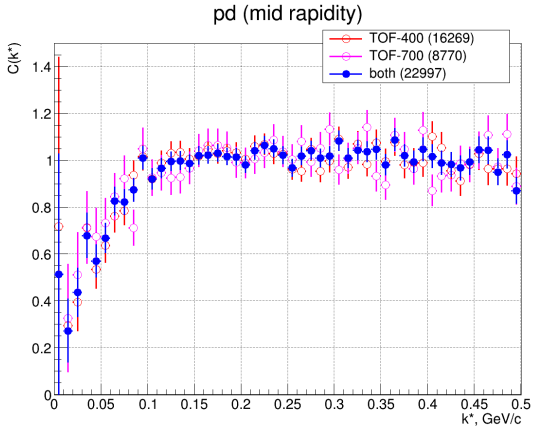

Fig.7.1. The experimental pd correlation functions in the midrapidity interval.

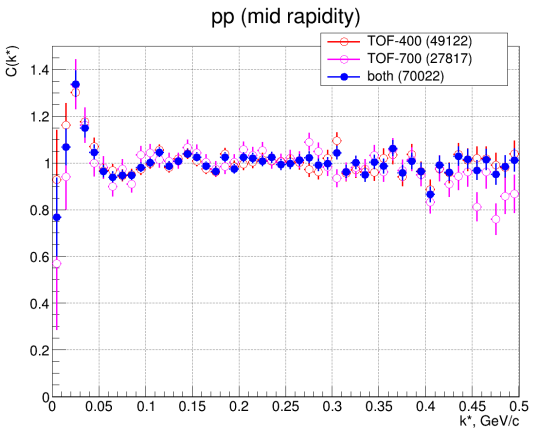

Fig. 7.2 The experimental pp correlation functions in the midrapidity interval.

8. Monte-Carlo simulations of the detector resolution and efficiency

To take into account the effects of the detector resolution and efficiency on the measured correction function, we started with the following procedure:

- events were generated within the framework of the DCM SMM model;
- particle pairs (pp, pd) in each event are stored with a theoretical correlation weight, assuming different sizes of the particle production region;
- the event particles then pass through the detector and undergo the standard reconstruction procedure;
- new values of the relative momentum are calculated for the particle pairs (pp, pd) to construct the distorted correlation function using the stored pair weight.

However, it turned out that without introducing the FSI and QS correlation weights into the model, there are already some correlations at small relative momenta (Fig. 8.1 (pd), 8.2 (pp)). E.g., they may result from a partial account of the FSI (for example, the Coulomb interaction in the final state). The depletion in the region of small relative momenta can be also a consequence of the oversimplified classical coalescence algorithm removing the coalescing nucleons with close three-momenta.

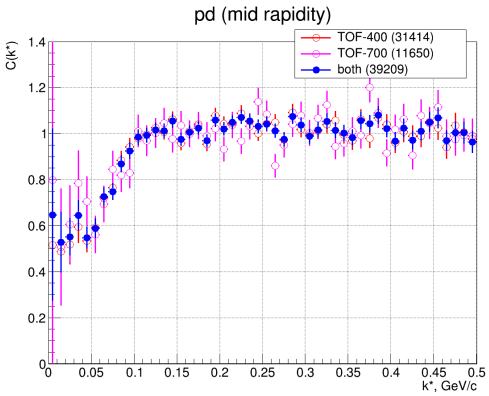

Fig.8.1 Correlation function of protons and deuterons in the DCM-SMM model

To eliminate the uncontrolled correlations in the model, a compensating weight was introduced for each pair of particles before introducing the theoretical (FSI+QS) correlation weight and then the reconstruction procedure was carried out.

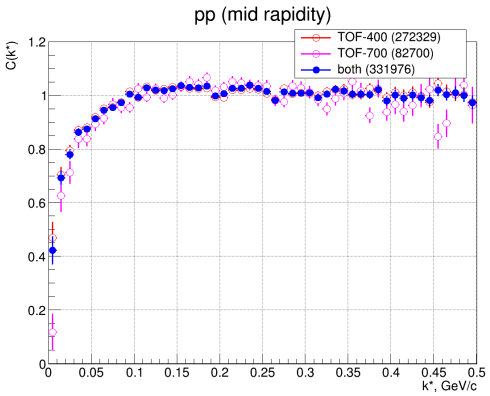

Fig.8.2 Proton correlation function in the DCM-SMM model

This approach is rather complicated and suffers from large fluctuations of the reconstructed theoretical correlation functions due to limited statistics of the simulated events. Therefore, another method was used, substituting the uncorrelated distributions of the pd and pp pairs by those obtained with the mixing procedure. It thus overcomes the problem of the limited statistics, though overlooking the effect of the two-track resolution at very small relative momenta.

Figures 8.3 (for pp) and 8.4 (pd) show the correlation functions before and after applying this procedure for different effective source radii r_0. The theoretical correlation function is shown in blue, and the result of its distortion by the setup (central range of rapidities) is shown in other colors.

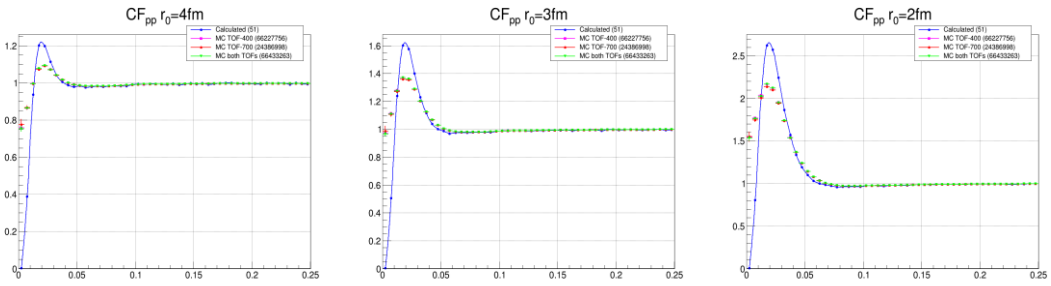

Fig.8.3 The two-proton correlation functions for the effective source radii r_0 = 2, 3, 4 fm (from left to right). The theoretical correlation function is shown in blue, other colors show the result of its distortion by the setup (central range of rapidities)

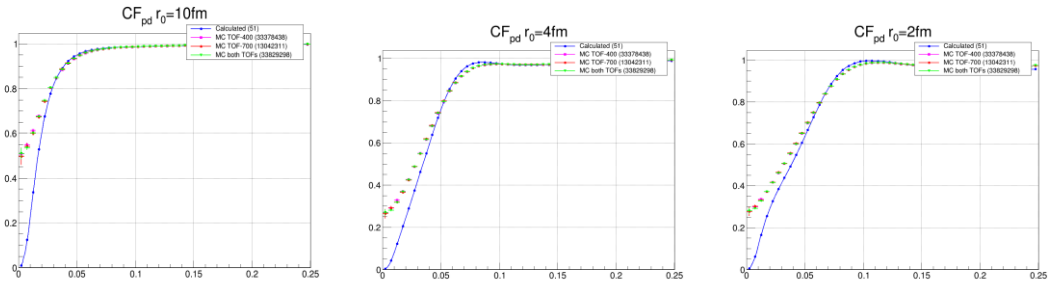

Fig.8.4 The proton-deuteron correlation functions for the effective source radii r_0 = 2, 4, 10 fm (from left to right). The theoretical correlation function is shown in blue, other colors show the result of its distortion by the setup (central range of rapidities)

9. Space-time parameters of the particle production region

The results of fitting the experimental proton-deuteron correlation function by the distorted theoretical ones are shown in Fig. 9.1.

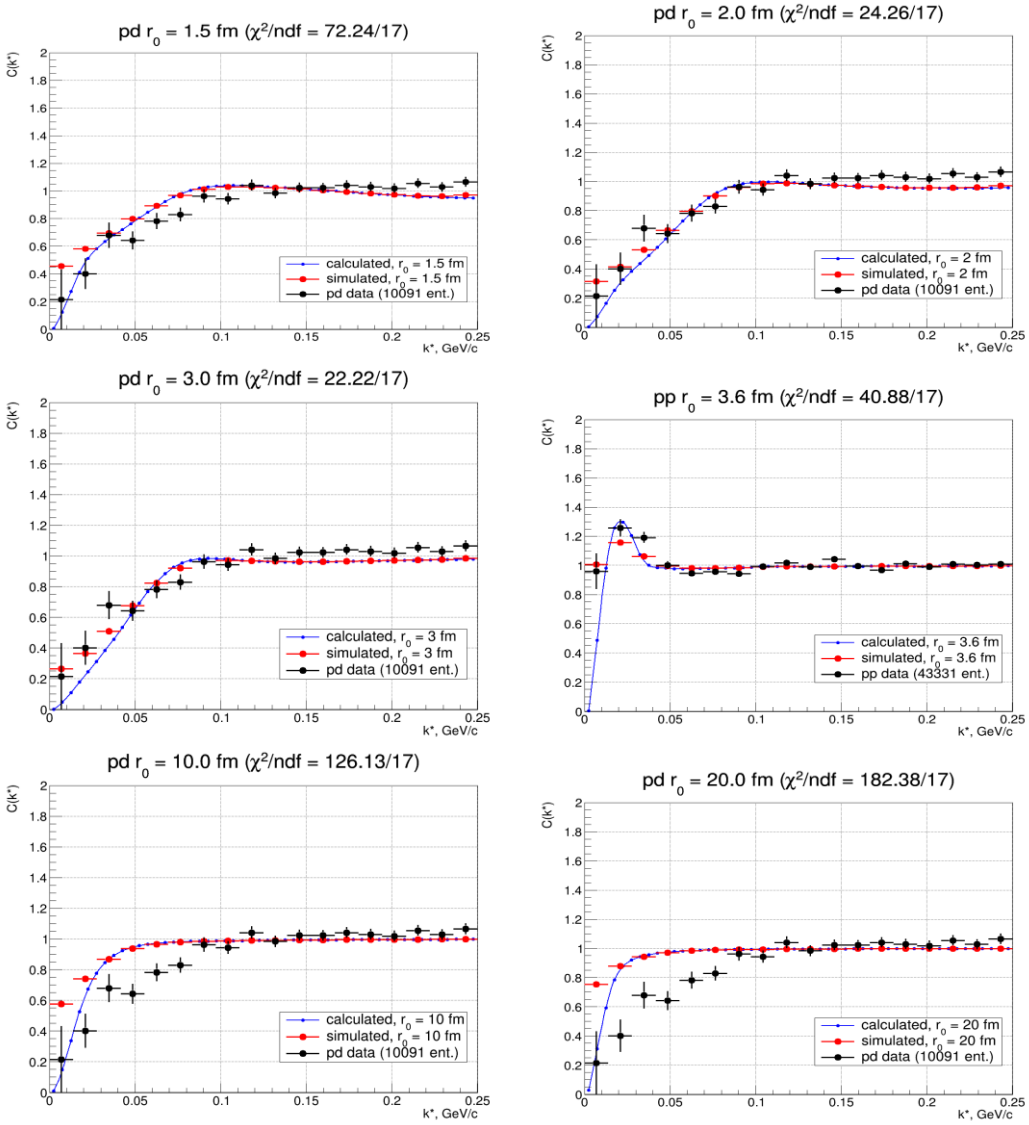

Fig. 9.1

The obtained values of χ^2 as a function of the effective source radius r_0 are shown in Fig. 9.2

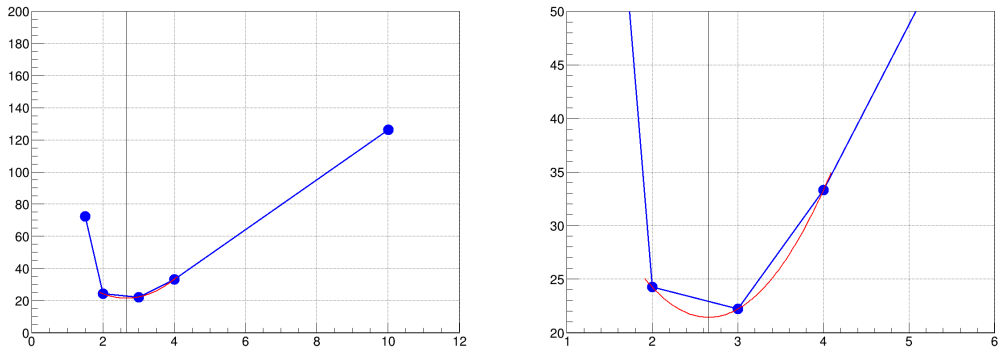

Fig. 9.2

Based on the obtained χ^2 values, the effective source radius estimated from proton-deuteron correlations is r_0 = 2.7+0.1-0.2(stat.) ±0.1(syst.) fm.

The results of fitting the experimental correlation function of two protons to theoretical curves taking into account the experimental resolution are shown in Fig. 9.3.

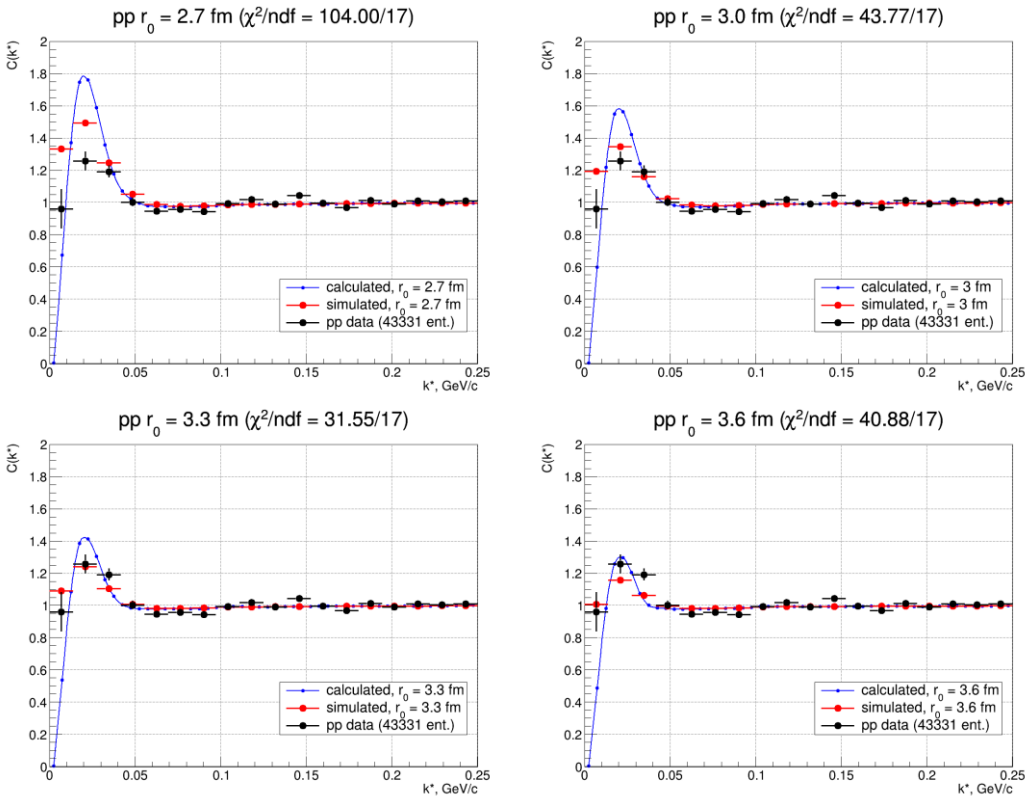

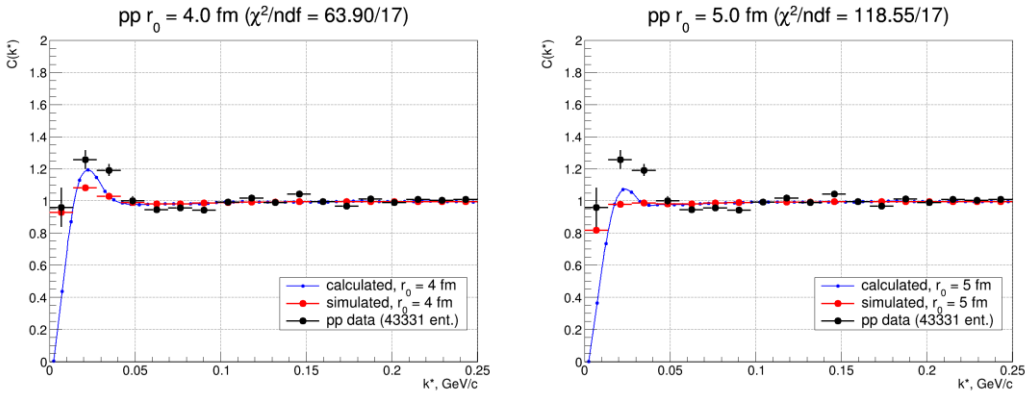

Fig. 9.3

The obtained values of $\chi 2$ as a function of the effective source radius r_0 are shown in Fig. 9.4.

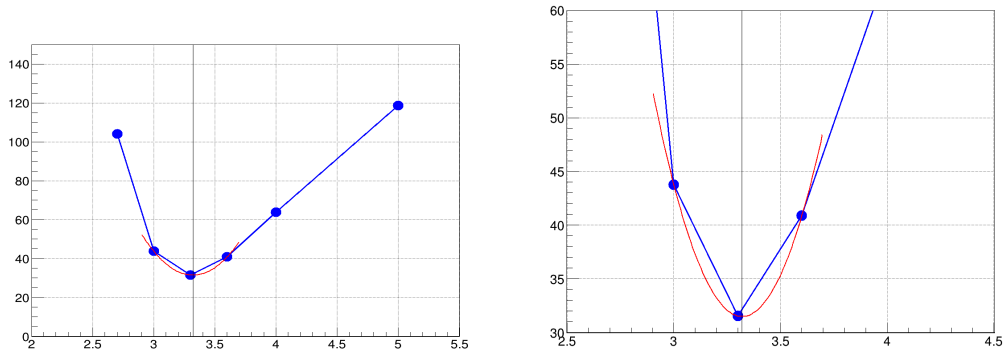

Fig.9.4

Based on the obtained χ^2 values, the effective source radius estimated from two-proton correlations is r_0 = 3.3±0.1(stat.)±0.1(syst.) fm.

10.Comparison with existing data

Figure 10.1 (Fig. 5 from the original paper) shows a selection of the effective source radii from [3]. The radii of ~3 fm obtained from two-proton correlations in the collisions of the nuclei of moderate atomic numbers are in good agreement with our results.

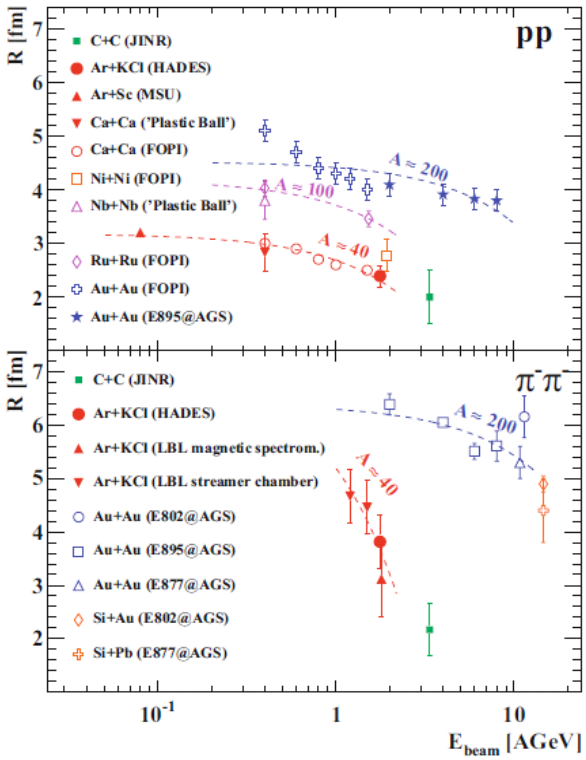

Fig. 5. (Color online) Top: The Gaussian source radius as derived from pp correlation functions in symmetric central heavy-ion collisions as a function of beam energy. The full red circle represent the HADES data. The other symbols given in the legend correspond to data of JINR [35], MSU [36], Plastic Ball [37], FOPI [14–17], E895 [38,39]. The various dashed curves are linear regressions to the data of the collision systems with sizes of $A + A \simeq 40 + 40$, $100 + 100$, and $200 + 200$. Bottom: The same, but for $\pi^-\pi^-$ correlation radii and for collision systems of size $A+A \simeq 40+40$ and $200+200$ (also including a few asymmetric systems). Further references: JINR [35], LBL magnetic spectrometer [40], LBL streamer chamber [41], BNL experiments E802 [42], E895 [43,39], E877 [44].

Fig. 10.1.

One may compare the fitted femtoscopic radii with those obtained within the coalescence model from the BM@N data on the light-ion production, also pointing to the nucleon source radius of ~3 fm [11].

	A	A^1/3	R^d_{coal}(pT = 0), fm*
Ar	**40**	**3,4**	
Al	27	3,0	2.7 ± 0.3
Cu	63	4,0	2.5 ± 0.2
Sn	120	4,9	2.8 ± 0.2
Pb	208	5,9	3.1 ± 0.2

11. Summary

Preliminary analysis of the proton-proton and proton-deuteron femtoscopic correlation functions obtained for particles produced with central rapidities in the interactions of the argon beam of 3.2 AGeV kinetic energy with various nuclei from carbon to lead indicate the proton and deuteron source size of about 3 fm.
Such a source size is in a good agreement with the results of the other femtoscopic correlation measurements under comparable conditions, as well as, sizes deduced within the coalescence model from the light-ion production.
A reasonable accuracy of the results obtained at moderate statistics of the argon run points to a good prospect of the femtoscopic studies of the spatio-temporal picture of the particle production in heavy-ion collisions planned at the BM@N facility with much higher statistics.

Bibliography

1. Kopylov G.I. Like particle correlations as a tool to study the multiple production mechanism // Phys. Lett. B 1974. V. 50. P. 472–474.
2. R Kotte et al. (The FOPI Collaboration) Eur. Phys. J. A 6, 185-195, 1999.
3.HADES G. Agakishiev et al. (HADES Collaboration) pp and $\pi\pi$ $\pi\pi$ intensity interferometry in collisions of Ar+KCl at 1.76A GeV // Eur. Phys. J. A (2011) **47**: 63
4. Aboona B.E. et al. [STAR Collaboration] Light nuclei femtoscopy and baryon interactions in 3 GeV Au+Au collisions at RHIC // Phys. Lett. B – 2025. V. 864. – P. 139412-1-8. – arXiv:2410.03436 [nucl-ex].
5. Acharya S. et al. [ALICE Collaboration] Femtoscopic study of the proton-proton and proton-deuteron system in heavy-ion collisions at the LHC // arXiv:2505.01061 [nucl-ex].
6. Podgoretsky M.I. Interference correlations of identical pions. Theory. // Sov. J. Part. Nucl. 1989. V. 20. P. 266–282.
7. Lednicky R., Podgoretsky M.I. The interference of identical particles emitted by the sources of different size // Sov. J. Nucl. Phys. 1979. V. 30. P. 432-439; Yad. Fiz. 1979. V. 30. P. 837-844.
8. Wang F. Residual correlation in two-proton interferometry from lambdaproton strong interactions // Phys. Rev. C 1999. V. 60. P. 067901-1-3. arXiv:nucl-th/9907032.
9. Stavinskiy A., Mikhailov K., Erazmus B., Lednicky R. Residual correlations between decay products of $\pi^0\pi^0$ $\pi^0\pi^0$ and $p\Sigma^0 p\Sigma^0$ systems // arXiv:0704.3290 [nucl-th].
10. Adamczyk L. et al. [STAR Collaboration] Measurement of Interaction between Antiprotons // Nature 2015. V. 527. P. 345–348. arXiv:1507.07158 [nucl-ex].
11. The BM@N collaboration., Afanasiev, S., Agakishiev, G. et al. Production of protons, deuterons and tritons in argon-nucleus interactions at 3.2 A GeV. J. High Energ. Phys. 2025, 95 (2025). https://doi.org/10.1007/JHEP08(2025)095